JGR Atmospheres

Impact of Cloud Microphysics Schemes on Tropical Cyclone Forecast Over the Western North Pacific

Jinyoung Park[1], Dong-Hyun Cha[1] (iD), Min Kyu Lee[1], Jihong Moon[1], Sook-Jung Hahm[2], Kyoungjo Noh[2], Johnny C. L. Chan[3] (iD), and Michael Bell[4] (iD)

[1]School of Urban and Environmental Engineering, Ulsan National Institute of Science and Technology, Ulsan, South Korea, [2]Weather Unit, 10th Fighter Wing, Republic of Korea Airforce, Gyeryong, South Korea, [3]School of Energy and Environment, City University of Hong Kong, Kwoloon, Hong Kong, [4]Department of Atmospheric Science, Colorado State University, Fort Collins, CO, USA

Abstract In high-resolution numerical modeling, cloud microphysics schemes can affect the forecasting of tropical cyclones (TCs) by controlling the phase changes of water. The simulated TC characteristics such as motion, intensity, and structure can change depending on the number of hydrometeors used in these schemes. In this study, we investigate the sensitivity of real-time track and intensity forecasts of TCs to cloud microphysics schemes using the Weather Research and Forecasting (WRF) model. For the sensitivity test, we selected WRF-single-moment-microphysics Class 3 (WSM3) and Class 6 (WSM6) schemes as simple and sophisticated schemes, respectively. A total of 20 forecasts for 10 TCs were conducted. For TCs moving westward in the subtropics, track forecasts were similar in the different sensitivity tests, although the WSM6 scheme considerably reduced the TC intensity errors. However, for TCs moving to the midlatitudes, the WSM6 scheme improved both track and intensity prediction compared to the WSM3 scheme. Particularly, track errors were prominently reduced by the WSM6 scheme, which realistically captured westward shifted track during the rapid intensification process. This can be attributed to the improved simulations of TC intensity, size, and associated β effect by WSM6 scheme. In contrast, the WSM3 scheme underestimated the above characteristics due to low latent heat release compared to the WSM6 scheme. Consequently, TC track moving northwestward was unreasonably shifted eastward. This indicates that a sophisticated cloud microphysics scheme is necessary to improve the track and intensity forecasts for TCs moving to the midlatitudes.

1. Introduction

Tropical cyclones (TCs) are one of the major meteorological hazards developing in the western North Pacific (WNP). Mature TCs are characterized by low pressure in the vicinity of the center, strong winds in the eye-wall, spiral rain bands, and torrential precipitation. In particular, landfalling TCs can trigger enormous economic loss and damage to the coastal regions (Knabb et al., 2006). Further, several studies have indicated a potential increase in the intensity of future TCs due to global warming, which may trigger more devastating natural disasters (Kitoh et al., 2009; Knutson et al., 2010). Thus, highly accurate TC forecasting is urgently required to save human resources and reduce economic losses in the future. Accordingly, several studies have focused on TC modeling to improve the accuracy of forecast (Mohanty et al., 2010; Rao & Rao, 2003; Srinivas et al., 2007). Despite the increasing model resolution (Miyoshi et al., 2010) and implementation of other techniques such as bogussing of initial TC vortex (Cha & Wang, 2013; Liu & Tan, 2016; Miguez-Macho et al., 2005), nudging large-scale fields (Cha et al., 2011; Liu & Xie, 2012; Moon et al., 2018), and improving physical parameterization schemes (Chatterjee et al., 2008; Zhang et al., 2012), the average position error of 24 hr TC forecast for the WNP region was about 59 km from the European Centre for Medium-Range Weather Forecasts (ECMWF) Integrated Forecast System (IFS) in 2018 (Chen et al., 2019), which was still a crucial concern in many coastal regions (Leroux et al., 2018).

It is challenging to represent subgrid-scale processes such as deep convection in simulation modeling (Stensrud, 2009; Warner, 2010). Due to the limited resolution of most numerical models, they have been implemented using various physical parameterization schemes. Hence, a higher horizontal resolution is crucial to resolve the small-scale processes associated with the formation of convective systems. Several studies have focused on high-resolution models to simulate TC structure, intensification, and movement with

different physical processes. Chutia et al. (2019) demonstrated that the horizontal resolution of prediction models is beneficial to simulate the TC track. The simulation of TC with 4 km horizontal resolution captured the patterns of the observed track, which were not realistically obtained in that with 9 km horizontal resolution.

Further, in high-resolution numerical modeling, cloud microphysics schemes can play a vital role in TC forecasting by controlling the phase changes of water within clouds and subsequent latent heat release (Chen et al., 2007; Nolan et al., 2009; Zou et al., 2010). Simulated TC structure can be affected by the number of hydrometeors used in such schemes. The latent heat released in the convective clouds depends on the microphysical processes, and it can facilitate a warm-core structure in the eye, which is essential for the development and maintenance of the circulations of TCs (Deshpande et al., 2012). Several earlier studies have evaluated the sensitivity of TC track and intensity forecast to cloud microphysics schemes. Zhu and Zhang (2006) examined the effect of various cloud microphysical processes on the intensity, precipitation, and inner-core structure of Hurricane Bonnie (1998) with triply nested (36/12/4 km) cloud-resolving fifth-generation Pennsylvania State University-National Center for Atmospheric Research Mesoscale Model (PSU-NCAR MM5). They showed that the weakest and shallowest storm was produced when ice microphysical processes were removed in the model. Further, they found that in the presence of graupel, the simulated hurricane became narrower and more intensified due to the rapid fallout of graupel in the eyewall, which helped to reduce water loading and facilitated the growth of updrafts and latent heat release. Consequently, they showed that the variation of cloud microphysical processes affected not only the intensity and intensity variations of the simulated TCs but also the changes in their inner-core structure. Pattnaik and Krishnamurti (2007) conducted a cloud microphysics sensitivity experiment with high-resolution (4 km innermost domain) MM5 to investigate the effect of different microphysical parameters on the intensity of Hurricane Charley in 2004. They showed that the microphysical processes (i.e., melting and evaporation) among hydrometeors and associated feedback mechanisms (i.e., fall speed and intercept parameter) significantly modulated the simulated hurricane intensity. Further, they found that the most intense storms were primarily simulated in the experiments where the melting of solid- and liquid-type hydrometeors and evaporation of rainwater were eliminated in the parameterization scheme. Furthermore, they confirmed that the increase in moist static energy facilitates the enhanced convection and its organization in the eye wall. Tao et al. (2011) tested and compared cloud microphysics schemes with triply nested (15/5/1.7 km) Weather Research and Forecasting (WRF) model for Hurricane Katrina in 2005 and found that the variations in such schemes can significantly impact the inner core structure of the storm. More compact eyewall structure with heavier precipitation, more symmetrical structures around the eye, and stronger warm cores tended to be simulated in stronger storms. Chan and Chan (2016) investigated the sensitivity of TC simulation to microphysics schemes with triply nested (36/12/4 km) WRF model. They found that the simulated TC intensity and size were enhanced when higher diabatic heating was generated in the spiral rainbands outside the eyewall. All these studies indicated that the cloud microphysical parameterization schemes had a substantial impact on the intensity prediction of TC but their effect on track forecast was not significant.

Until now, very few modeling studies have investigated the impact of cloud microphysics schemes on TC forecasting using high-resolution (about 5 km or less) numerical models. In addition, most of these studies did not implement real-time forecasting because they used reanalyzed or analyzed data as initial and boundary conditions and their results were mostly confined to a few TC cases. To this end, in this study, we investigate the sensitivity of real-time track and intensity forecasts of TCs to cloud microphysics schemes using the WRF model. In particular, WRF-single-moment-microphysics Classes 3 and 6 (WSM3 and WSM6) schemes are selected as simple and sophisticated cloud microphysics schemes for implementing warm rain processes and cold rain processes, respectively. A total of 20 forecasts for 10 TCs that occurred from 2012 to 2018 were conducted using a high-resolution (2 km for core region) WRF model with the moving nesting method.

Overall, the objective of this study is to understand the effect of cloud microphysics schemes on the real-time forecast of track, intensity, and structure of TCs over the WNP region. The rest of this paper is organized as follows. Section 2 describes the model configuration and experimental design. The simulation results are presented in section 3. Section 4 concludes the study.
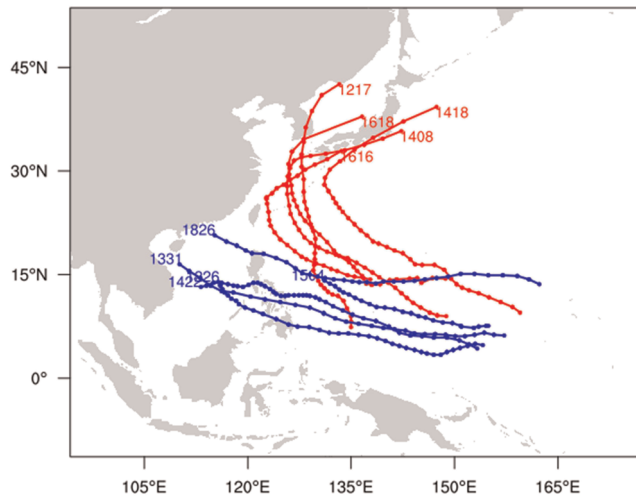
Figure 1. JTWC best tracks for the all simulated TC cases at the 6 hr intervals. The blue and red lines represent the westward and northwestward moving TCs, respectively.

2. Model Configuration and Experimental Design

WRF model (Skamarock et al., 2008) Version 3.7.1 was used as the regional model. The initial and boundary conditions were obtained from the 0.5° × 0.5° real-time forecast data of National Centers for Environmental Prediction (NCEP) Global Forecasting System (GFS). Similar to the model setup of Cha and Wang (2013), our model consisted of three domains with 18 km (341 × 271), 6 km (331 × 331), and 2 km (211 × 211) horizontal resolutions (grid points). We used the two-way moving nesting technique for Domains 2 and 3 to rationally resolve the inner core structure of TC. The domain contained 35 vertical levels from the surface to the top of the atmosphere at 50 hPa. The model utilized the WSM3 and WSM6 cloud microphysics schemes (Hong et al., 2004; Hong & Lim, 2006), Yonsei University planetary boundary layer scheme (Hong et al., 2006; Noh et al., 2003), Dudhia short-wave radiation scheme (Dudhia, 1989), and long-wave radiation scheme based on rapid radiative transfer model (Mlawer et al., 1997). Kain-Fritsch scheme (Kain, 2004) was only employed for convective processes in domain 1 with 18 km resolution.

The WSM3 and WSM6 cloud microphysics schemes were selected for the sensitivity experiments (hereafter called WSM3 and WSM6 runs, respectively). The WSM3 scheme is a simple-ice scheme, which considers only three variables of prognostic water substance including mixing ratios of water vapor, cloud water/ice, and rainwater/snow. In this scheme, cloud water and rainwater, whose mixing ratios are calculated by diagnostic equation, are assumed to exist above 0°C. Further, they are considered as ice and snow below 0°C. This scheme is widely used in real-time global or regional models, as it consumes less computational resources than other microphysics schemes (Liang et al., 2012; Mooney et al., 2013). The WSM6 scheme is similar to the WSM3 scheme. However, WSM6 scheme is a more sophisticated scheme than WSM3 scheme because it considers three additional prognostic hydrometeors (i.e., snow, ice, and graupel) and includes more complicated processes associated with the phase change among them. WSM3 scheme only predicts the liquid phase variables, and supercooled water is not considered because liquid phase variables cannot coexist with the solid phase variables. Further, it does not consider the variable of solid-type water substance, that is, mixing ratio for graupel. Therefore, the characteristics of simulated TC can be different in the two schemes.

For the sensitivity experiments, we selected 10 TC cases in the WNP region that occurred from 2012 to 2018 (Figure 1). These cases were divided into two groups according to the direction of the TC movement; five cases included westward moving TCs in the subtropical region, and the remaining included northwestward moving TCs from the subtropics to the midlatitudes. Further, we conducted two forecasts with different initial times for each TC, and the initial forecast times were at least 24 hr before the TC attained lifetime maximum intensity because we wanted to understand the effect of cloud microphysics scheme on the track and intensity during the intensification stage of TC. Thus, a total of 20 simulations for 10 TC cases were conducted. The initial forecast times, directions, and lifetime maximum intensities for all TC cases are shown in Table 1.

Similar to the study of Cha and Wang (2013), the center of outermost domain was 5° (7.5°) to the north (northwest) from the observed TC center if the latitude of the observed TC center was north (south) of 20°N, while the centers of the two nested domains were near the observed TC center. The integration time steps of the model for Domains 1–3 were 90, 30, and 10 s, respectively. The forecast runs were initialized at 0000 or 1200 UTC and integrated for 72 hr.

3. Results and Discussion

3.1. Track and Intensity Forecasts

The difference in TC track and intensity forecasts between the WSM3 and WSM6 runs was analyzed by calculating the forecast errors with respect to the best track data from Joint Typhoon Warning Center (JTWC). Track forecast error is defined as the great circle distance between the center position of a TC forecast and

Table 1
Initial Times, Directions, and Lifetime Maximum Intensities for the Simulated 10 TCs, Which Occurred From 2012 to 2018

TC number	TC name	Forecast initial time	Direction	Lifetime maximum intensity (time)
1217	Sanba	2012/09/12 1200 UTC 2012/09/13 0000 UTC	Northwestward	907 hPa (2012/09/14 00 UTC)
1226	Bopha	2012/11/30 0000 UTC 2012/11/30 1200 UTC	Westward	911 hPa (2012/12/03 18 UTC)
1331	Haiyan	2013/11/05 1200 UTC 2013/11/06 0000 UTC	Westward	895 hPa (2013/11/07 12 UTC)
1408	Neoguri	2014/07/05 0000 UTC 2014/07/06 0000 UTC	Northwestward	918 hPa (2014/07/07 00 UTC)
1418	Phanfone	2014/10/01 0000 UTC 2014/10/02 0000 UTC	Northwestward	922 hPa (2014/10/04 00 UTC)
1422	Hagupit	2014/12/03 0000 UTC 2014/12/03 1200 UTC	Westward	907 hPa (2014/12/04 00 UTC)
1504	Maysak	2015/03/29 0000 UTC 2015/03/30 0000 UTC	Westward	911 hPa (2015/03/31 12 UTC)
1618	Malakas	2016/09/14 0000 UTC 2016/09/15 0000 UTC	Northwestward	937 hPa (2016/09/16 12 UTC)
1621	Chaba	2016/10/01 0000 UTC 2016/10/02 0000 UTC	Northwestward	911 hPa (2016/10/03 06 UTC)
1826	Mangkhut	2018/09/09 0000 UTC 2018/09/10 0000 UTC	Westward	896 hPa (2018/09/12 06 UTC)

the best track position (Chen et al., 2013, 2016). Intensity forecast error is defined as the difference between the intensity forecast (i.e., maximum 10-m wind speed and minimum sea level pressure) and best track intensity at the forecast hour (Chen et al., 2016).

Figure 2 compares the track and intensity forecast errors of the WSM3 and WSM6 runs for each lead time level and their average value. Generally, for all TC cases, both track and intensity forecast errors tend to be lower in the WSM6 runs compared to those in the WSM3 runs. Further, TC intensities in the WSM3 run are prominently underestimated compared to that in the JTWC best track. It is noteworthy that the two groups show distinct aspects of track forecasts. For westward moving TCs, the differences in the average of track forecast errors between the two runs are smaller than those for northwestward moving TCs; differences in track forecast errors at 24, 48, and 72 hr forecast hours for westward moving TCs are 6.6, 10.3, and 13.9 km, while those for northwestward moving TCs are 15.7, 31, and 81.7 km, respectively. This implies that the track forecasts of westward moving TCs are less sensitive to the cloud microphysics scheme. On the contrary, for northwestward moving TCs, the differences in the track forecast errors between the two runs are relatively large and exhibit a significant increase with simulation hours. In contrast to the track forecast, intensity errors as well as their differences between the two runs in westward moving TCs are larger than that in northwestward moving TCs.

Figures 3 and 4 show the 3-day track and intensity forecast results in the sensitivity experiments for westward and northwestward moving TCs, respectively. Typhoons Bopha in 2012 and Maysak in 2015 are selected for westward moving TCs, and typhoons Malakas and Chaba in 2016 are chosen for northwestward moving TCs. As confirmed in Figure 2, westward moving TCs have similar track patterns in the WSM3 and WSM6 runs (Figures 3a and 3d), while northwestward moving TCs have a relatively large track difference (Figures 4a and 4d). For northwestward moving TCs, simulated track in the WSM6 run tends to move more northwestward compared to that in the WSM3 run. In contrast, intensity forecasts are quite similar in westward and northwestward moving TCs. In general, all simulated TCs in the WSM6 run are more rapidly intensified compared to those in the WSM3 run. Especially, their intensity differences are most prominent during the intensification period. It is noteworthy that the track difference between the sensitivity experiments tends to increase during the intensification period in northwestward moving TCs. In the case of Malakas, the track difference between the two runs increases after 42 hr forecast. Further, the largest difference in TC intensity between the two runs appears at the same forecast hour (i.e., 42 hr). These results for Malakas are similar to those for Chaba and for other TC cases in northwestward moving TCs. This indicates that the simulated TC track might be related to the intensity forecast in northwestward moving TCs. For
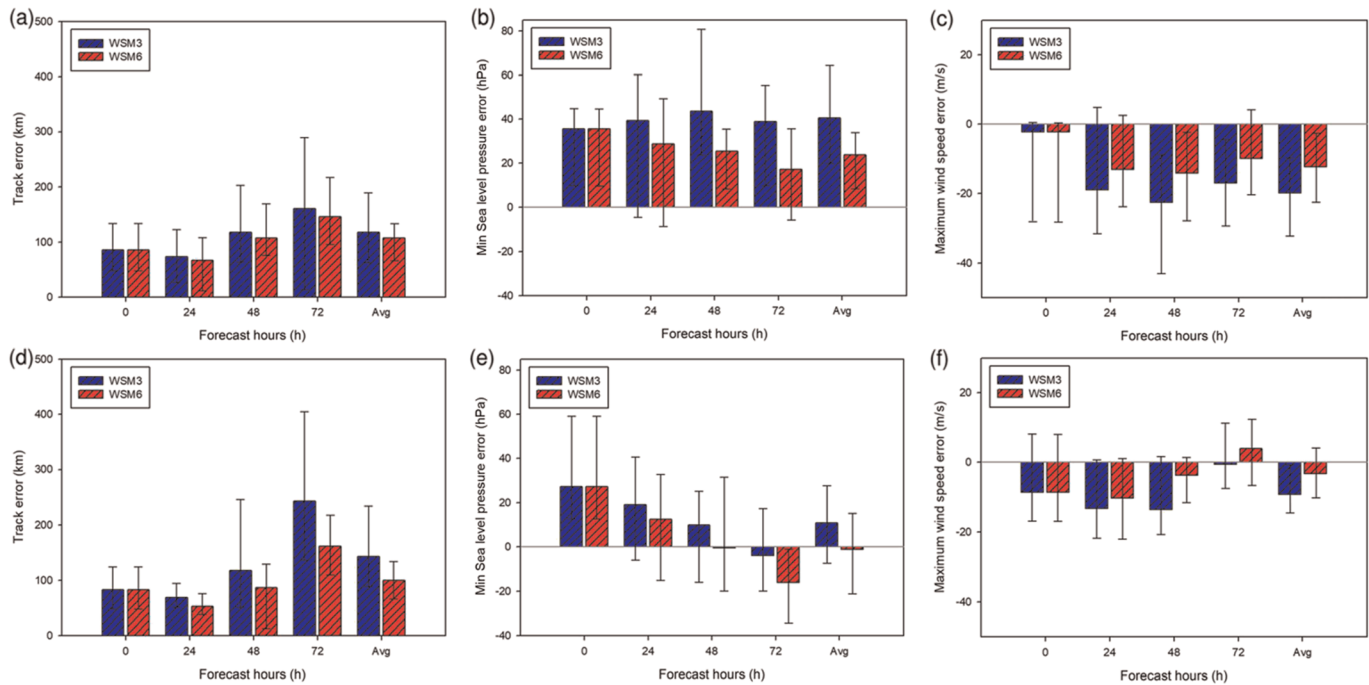
Figure 2. Mean forecast errors of (a, d) track (km), (b, e) minimum sea level pressure (hPa), and (c, f) maximum wind speed (m s^{-1}) at the 0, 24, 48, 72 hr forecast hours and total average. The upper and lower figure show the WSM3 (blue) and WSM6 (red) runs in westward and northwestward moving TCs, respectively. Error bars represent the spread between the maximum and minimum errors.

westward moving TCs, the intensity difference between the two runs and whether rapid intensification (RI) is captured or not may be less relevant to the track forecast.

To investigate the relationship between the intensity forecast and track forecast, we analyzed the cross- and along-track differences with respect to the intensity differences between the two runs. The cross-track error is defined as the absolute error in the component perpendicular to the best track of the TC. Also, the along-track error is defined as the component of the absolute error along the direction of the best track of the TC. To identify the differences in track forecast skill between the two runs, we compared the cross- and along-track differences of the WSM6 and WSM3 runs. The positive values of cross-track difference indicate that the simulated TC track in the WSM6 run is located on the right side of the WSM3 run. Also, the positive values of along-track difference indicate that the simulated TC in the WSM6 run moves faster than the WSM3 run. Overall, the cross-track difference between the two runs tends to increase with the forecast hour, as shown in Figure 5. For the forecast stage earlier than 12 hr, the cross-track difference between the two runs is nearly constant in both the groups, and the intensity difference between the two runs is not significant. Subsequently, the intensity difference and the cross-track difference between the two runs gradually increase in both the groups. However, the increasing trend of cross-track difference in northwestward moving TCs appears much earlier and is more prominent than that in westward moving TCs. At 72 hr forecast, the cross-track difference between the two runs for northwestward moving TCs is about −80 km, while that for westward moving TCs is around +40 km. The considerable negative cross-track difference in northwestward moving TCs implies that TC track in the WSM3 run is unreasonably shifted eastward compared to that in the WSM6 run. In contrast, the along-track difference between the two runs for both the groups does not vary significantly except in the late forecast stage, where it becomes slightly negative, indicating that the WSM6 run simulates somewhat slower movements of TCs than the WSM3 run (Figure 6). This can be attributed to the fact that TCs simulated with the WSM3 scheme experience more rapid weakening (most of them are weak enough to be considered as the tropical depression) compared to those simulated with the WSM6 scheme, especially during the late forecast stage.

These results show that the differences in simulated TC intensity between the WSM3 and WSM6 runs can be related to the track forecast for northwestward moving TCs. Simulated TCs in the WSM6 scheme undergo
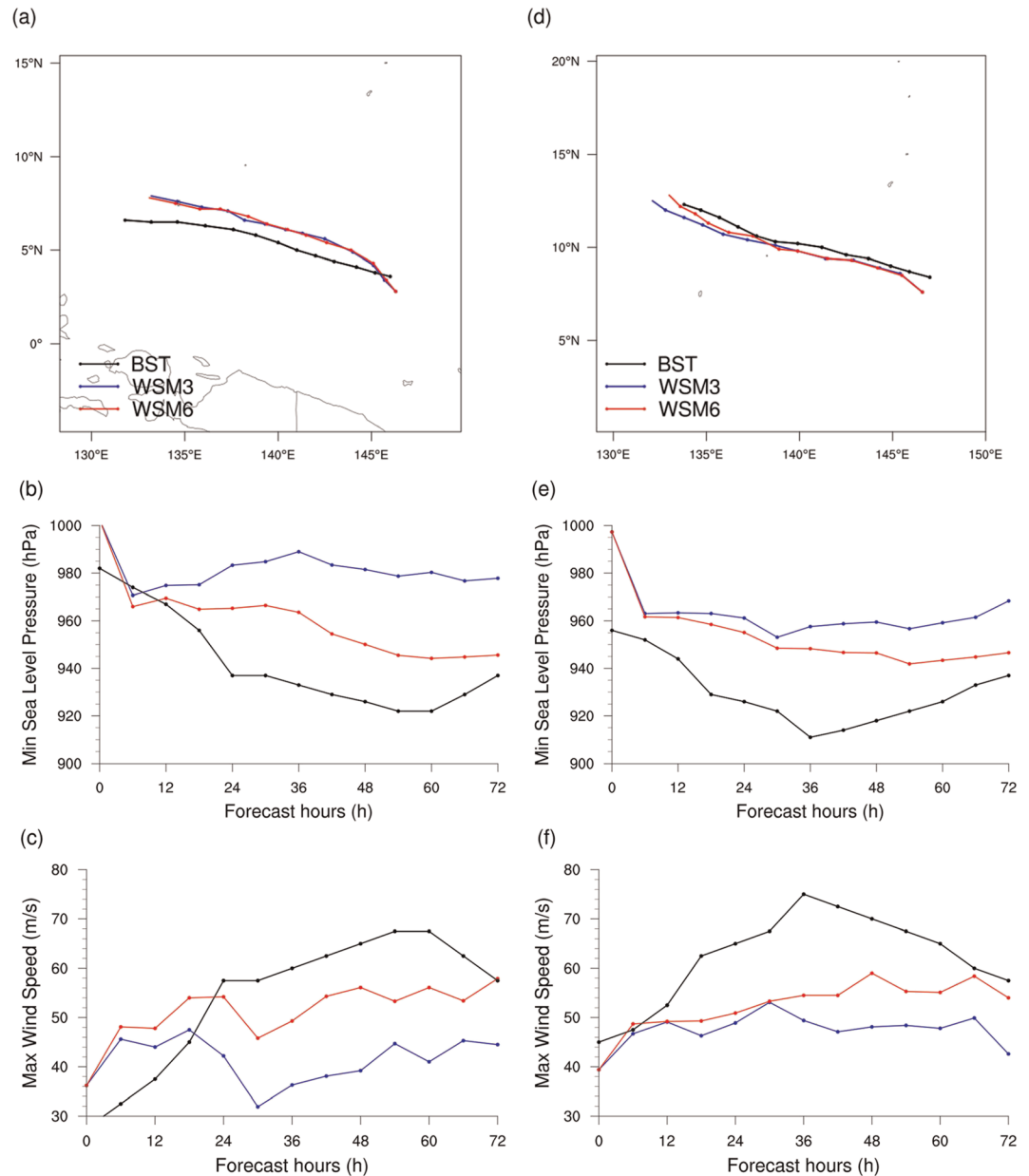
Figure 3. Simulated TC (a, d) track, (b, e) minimum sea level pressure, and (c, f) maximum surface wind speed in the WSM3 run (blue), WSM6 run (red), and best track (black) of westward moving TC Bopha (initialized at 0000 UTC 30 November 2012, left) and Maysak (initialized at 0000 UTC 30 March 2015, right).

rapid changes in intensity. In particular, TC tracks in northwestward moving TCs are relatively shifted northwestward by the WSM6 scheme compared to that by the WSM3 scheme. This may be related to the fact that the different β effect, which is also a function of TC size and intensity, causes the TCs to move northwestward in the Northern Hemisphere (Chan et al., 2002; Chan & Gray, 1982; Fiorino & Elsberry, 1989). To this end, we now analyze the reason for the differences in simulated TC intensities between the two runs by comparing the simulated TC structures.

3.2. Role of the Phase Variation of Hydrometeors

As the number of hydrometeor species considered and their distributions are different in the two schemes, the intensification process during the TC forecast can be different in the sensitivity experiments. To compare
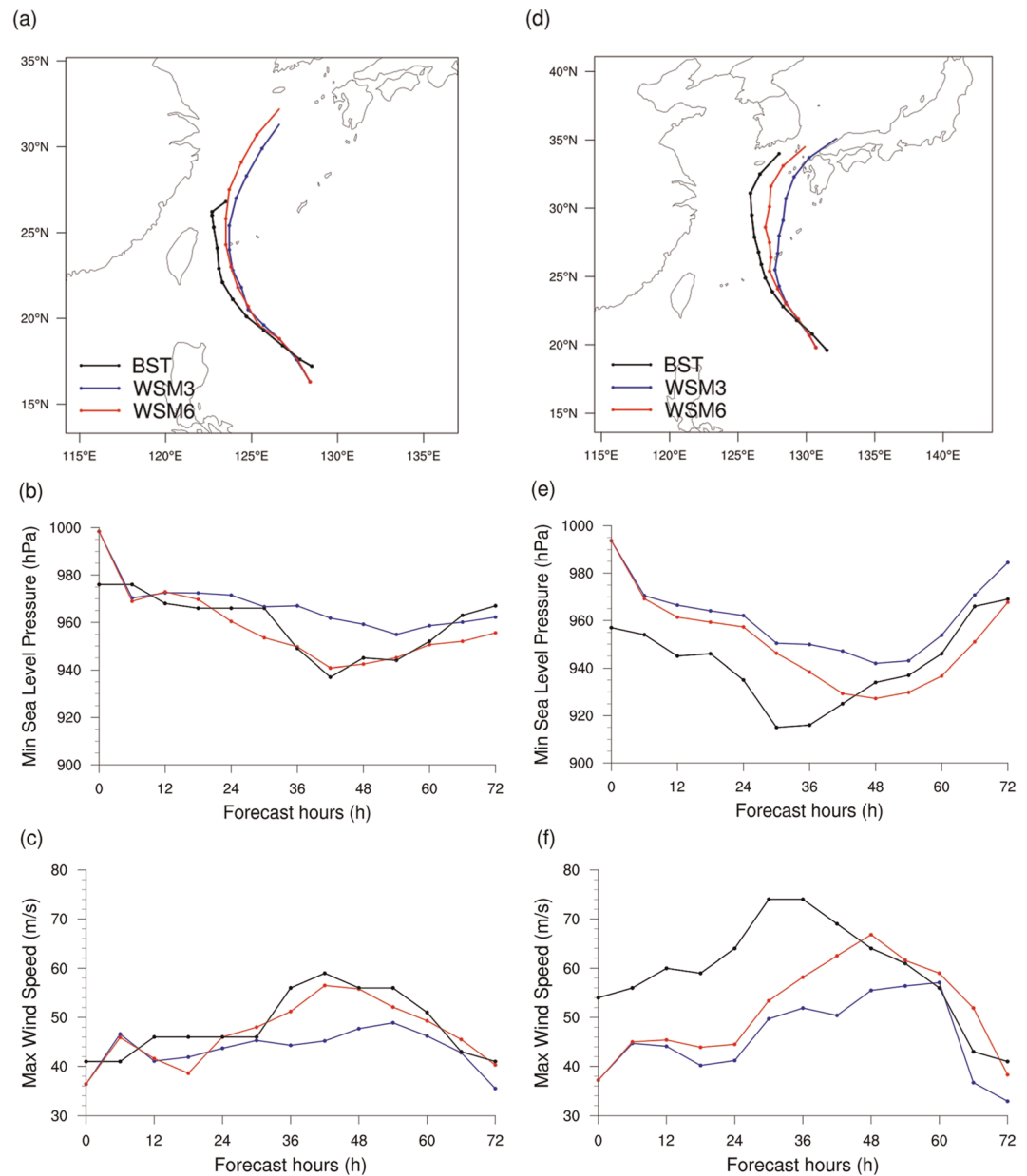
Figure 4. Same as Figure 3 but for the northwestward moving TC Malakas (initialized at 0000 UTC 15 October 2016, left) and Chaba (initialized at 0000 UTC 02 October 2016, right).

the differences in the inner-core structure of simulated TC between the two runs, we analyzed the three-dimensional structure of TC Malakas, which exhibited vertical-radial structure of the azimuthal mean of tangential and radial wind, temperature anomaly, and diabatic heating at the lifetime peak intensity (Figure 7) that is typical for well-developed TCs. The temperature anomaly was calculated as the azimuthal-mean temperature difference from the horizontal mean value within the radius of 4° from the TC center. In the WSM6 run, the intensity of simulated TC was much stronger, and the cloud top achieved a higher level compared to that in the WSM3 run. Despite the lifetime peak intensity in both the experiments, tangential and radial winds were prominently stronger, and simulated TC had slightly greater height and larger size in the WSM6 run than in the WSM3 run. Further, warm core structure was more enhanced at the upper level in the WSM6 run. The primary cause of the TC intensification is the release of latent heat in the inner core of the TC (Emanuel, 1986; Guimond et al., 2011). Here, the
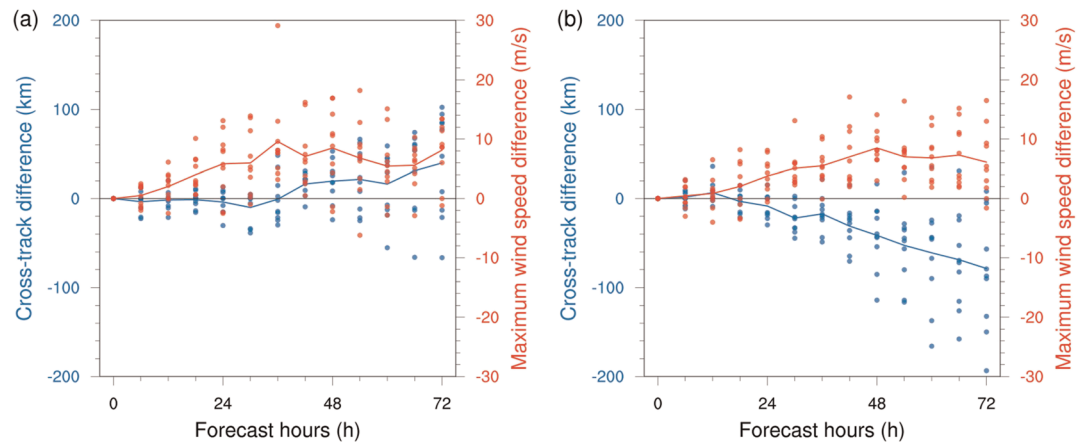
Figure 5. Scatterplot of cross-track difference (km, blue) and maximum intensity difference (m s^{-1}, red) of the WSM6 run against to the WSM3 run for (a) westward and (b) northwestward moving TCs. Solid blue and red lines indicate the mean cross-track difference and intensity difference, respectively.

atmospheric latent heat release around TC core regions was governed by the cloud microphysical processes because cumulus parameterization scheme was not employed in Domains 2 and 3. Thus, the difference in the intensification process between the WSM3 and WSM6 runs is related to different diabatic heat released from cloud microphysical processes.

To clarify the effect of different cloud microphysical processes in sensitivity experiments, we analyzed the vertical cross section of the cloud particles (i.e., cloud water and ice), precipitable particles (i.e., rain water, snow, and graupel), and potential temperature at the lifetime peak intensity of TC Malakas. Figure 8 shows that the overall distribution of the cloud and precipitable particles in the updraft region near the simulated TC center and upper-level clouds are reasonably simulated in both the runs. However, the detailed features of the upper-level hydrometeors between 100 and 400 hPa are significantly different in the two runs. As the WSM3 scheme includes only three variables of prognostic water substance, mixing ratios for cloud water and rainwater are considered as ice and snow, respectively, for temperature below 0°C. In contrast, the WSM6 scheme explicitly calculates three more prognostic variables (i.e., ice, snow, and graupel), which require additional computation time. In addition, the WSM6 scheme, which is a mixed-phase scheme, allows the existence of supercooled water. The supercooled water is involved in the process of growing of snow by riming of ice crystals and also helps forming of graupel by riming of snow. Therefore, warmer temperature at the middle and upper levels indicate that enhanced warm core is more effectively simulated by the WSM6
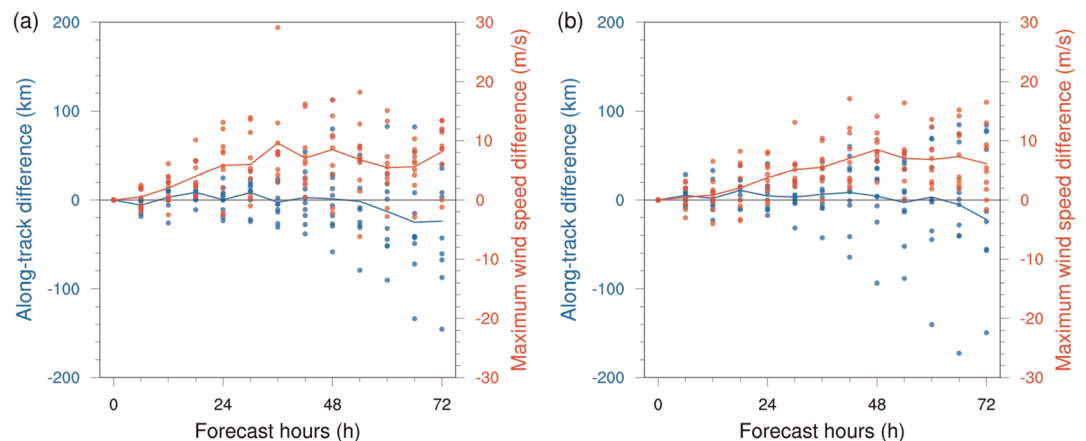

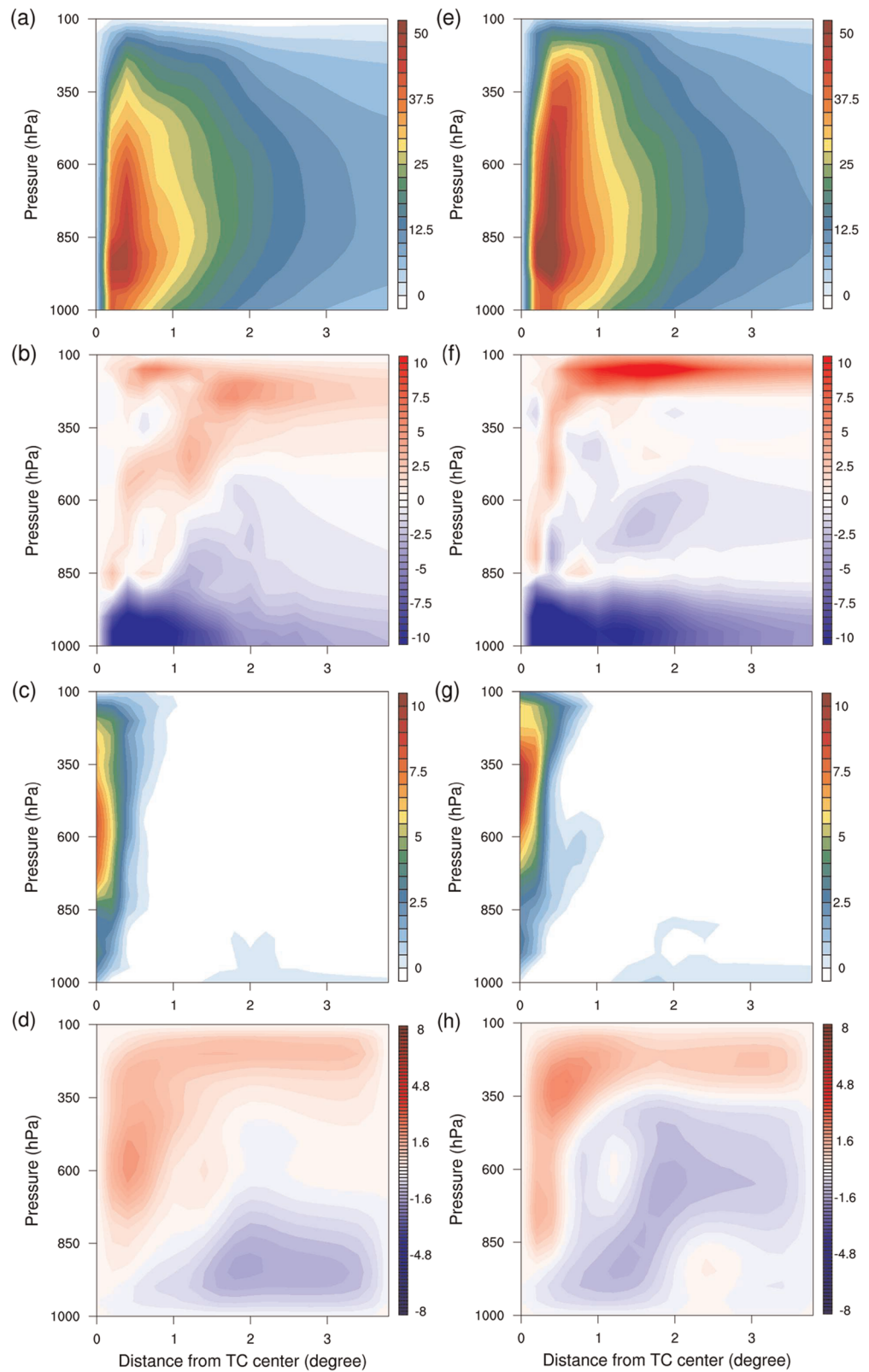**Figure 6.** Same as Figure 5 but for the along-track difference.

Figure 7. Vertical and radial structure of the azimuthal mean of (a, e) tangential wind (m s^{-1}), (b, f) radial wind (m s^{-1}), (c, g) temperature anomaly (K), and (d, h) diabatic heating (K day^{-1}) in the WSM3 run (left) at 0600 UTC 17 October 2016 (54 hr forecast) and WSM6 run (right) at 1800 UTC 16 October 2016 (42 hr forecast) in the 2 km domain for the northwestward moving TC Malakas. The initial forecast time is 0000 UTC 15 October 2016.
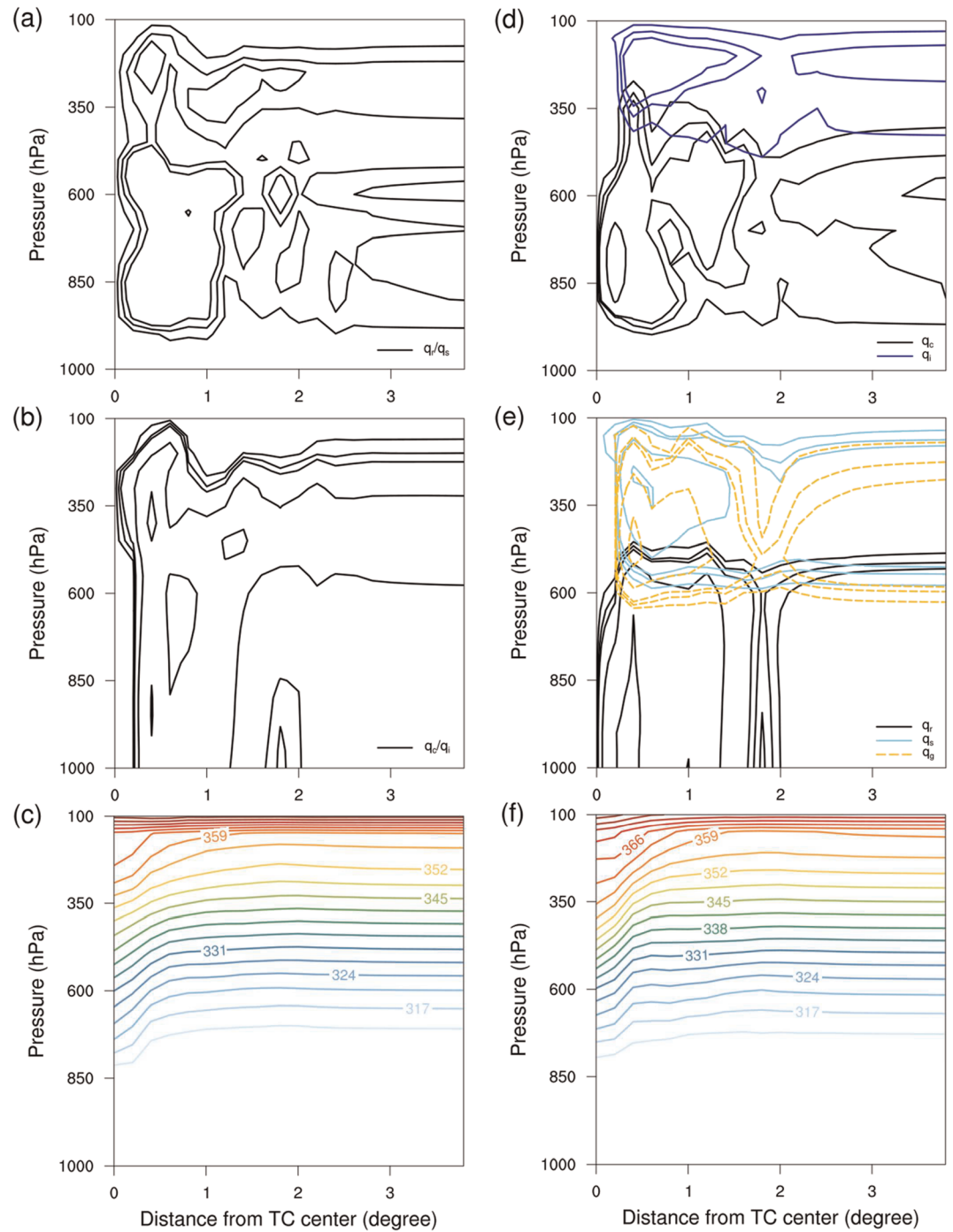
Figure 8. Vertical and radial structure of the azimuthal mean of (a, d) cloud particles, (b, e) precipitable particles, and (c, f) potential temperature (K) in the WSM3 run (left) at the 54 hr forecast and WSM6 run (right) at the 42 hr forecast in the 2 km domain for the northwestward moving TC Malakas. q_c, q_r, q_i, q_s, and q_g indicate cloud water, rain water, ice, snow, and graupel, respectively. Contour lines of hydrometeors are at 0.02, 0.05, 0.08, 0.3, 1.0, 2.5, and 5.0 g kg^{-1}, and the contour interval of potential temperature is 3.5 K. The initial forecast time is 0000 UTC 15 October 2016.

scheme than that by the WSM3 scheme. This implies that the impact of latent heat release at the middle and upper levels around the TC core region on the intensification process is more significant in the WSM6 scheme compared to that in the WSM3 scheme. The different latent heat release in the two schemes can
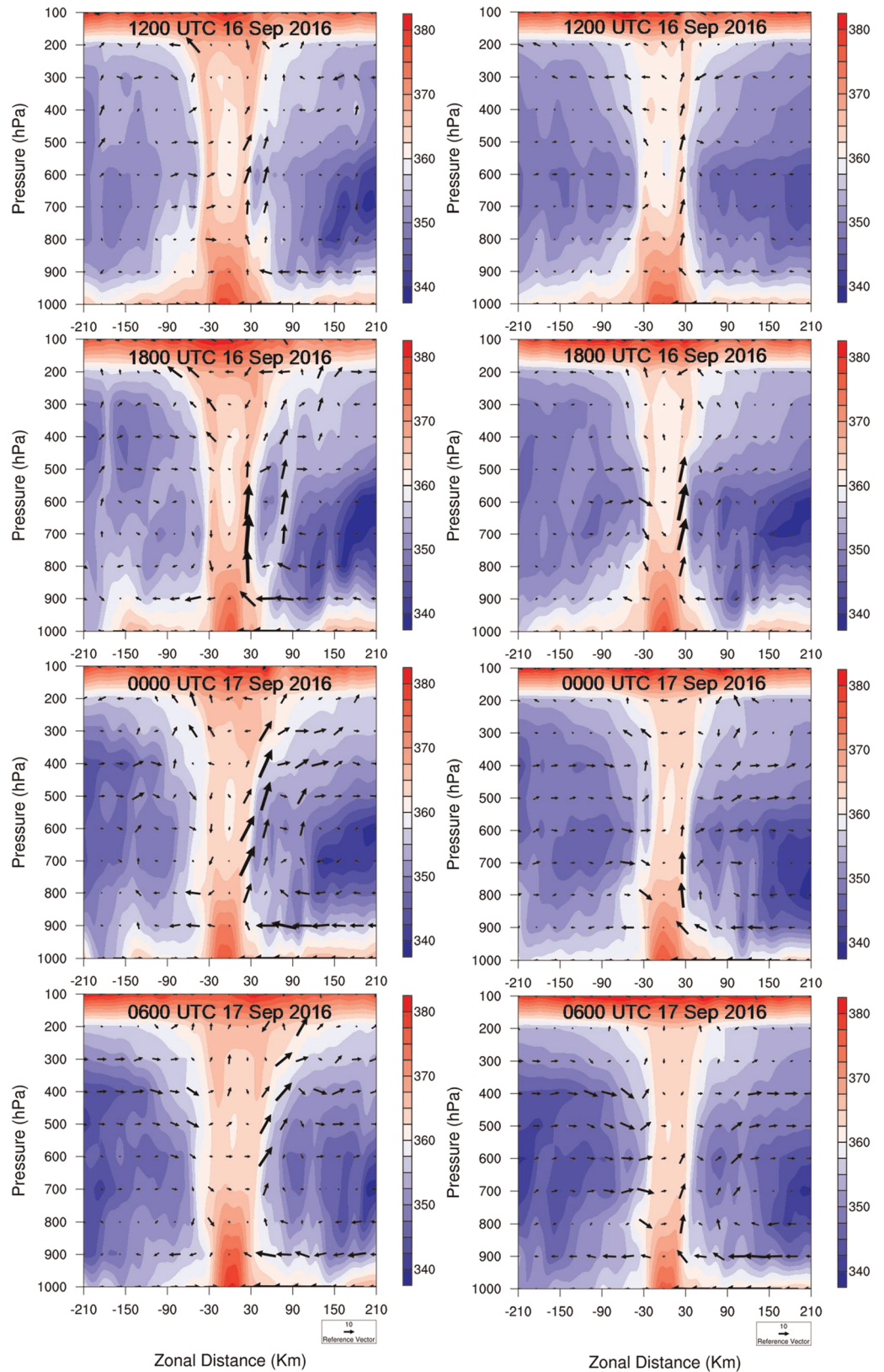
Figure 9. Vertical cross sections of equivalent potential temperature (shading, K) and wind fields (U and W × 10 components, vector) in the WSM3 (left) and WSM6 (right) runs in the 2 km domain at 6 hr intervals. The initial forecast time is 0000 UTC 15 October 2016 for the northwestward moving TC Malakas.
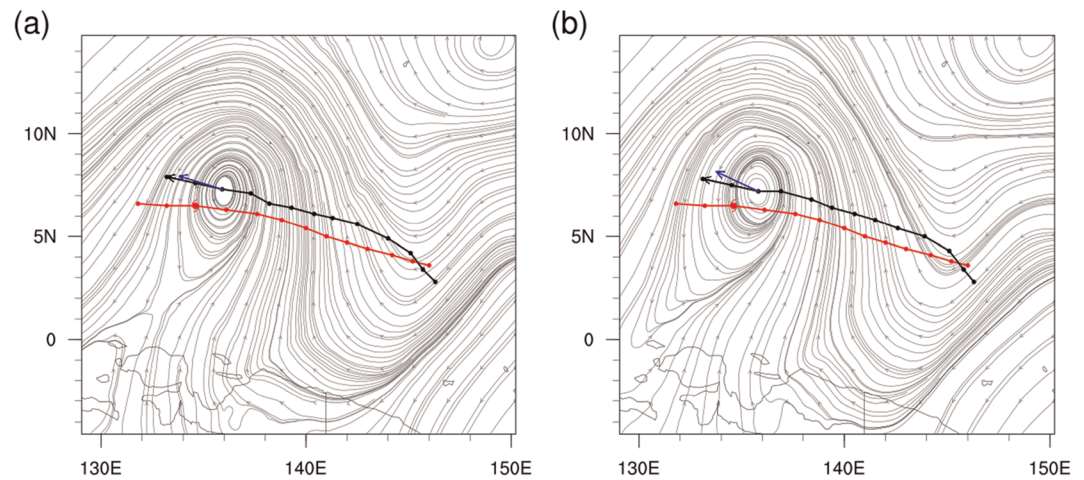
Figure 10. Streamlines averaged at 300–850 hPa, TC motion vector (black vector), and steering flow vector (blue vector) in the (a) WSM3 and (b) WSM6 runs for the westward moving TC Bopha at 1200 UTC 2 December 2012 (54 hr forecast). Red and black lines indicate TC tracks of the best track and simulations, respectively. TC mark represents the TC location of the best track at the forecast hour.

be attributed to more diabatic heating around the TC core region in the WSM6 scheme, which is primarily induced by the production of graupel (Kanase & Salvekar, 2015; Mukhopadhyay et al., 2011). The more enhanced upper-level warm core structure of the simulated TC in the WSM6 runs in Figure 7g is associated with the dry adiabatic descent within the eye and larger amount of vertically transported heat within the eyewall. These updrafts within the eyewall are accompanied by the latent heat release from condensation process. We also showed it in Figure 9. Figure 9 shows the 6 hourly evolution of intensification processes in the two runs at the lifetime peak intensity of TC Malakas. As the forecast hour increases, simulated two TCs are intensified with increased equivalent potential temperature at the upper-level, enhanced vertical motion; low-level inflow; upper-level outflow; and the low-level cyclonic circulation in the two runs. However, these processes are more prominently enhanced in the WSM6 run than that in the WSM3 run. Consistent with the studies of Mukhopadhyay et al. (2011) and Deshpande et al. (2012), more latent heat release at the middle and upper levels enhances the vertical motions in convective clouds, which leads to the intensification of the system by strengthening divergence at the upper level and convergence at the lower level.
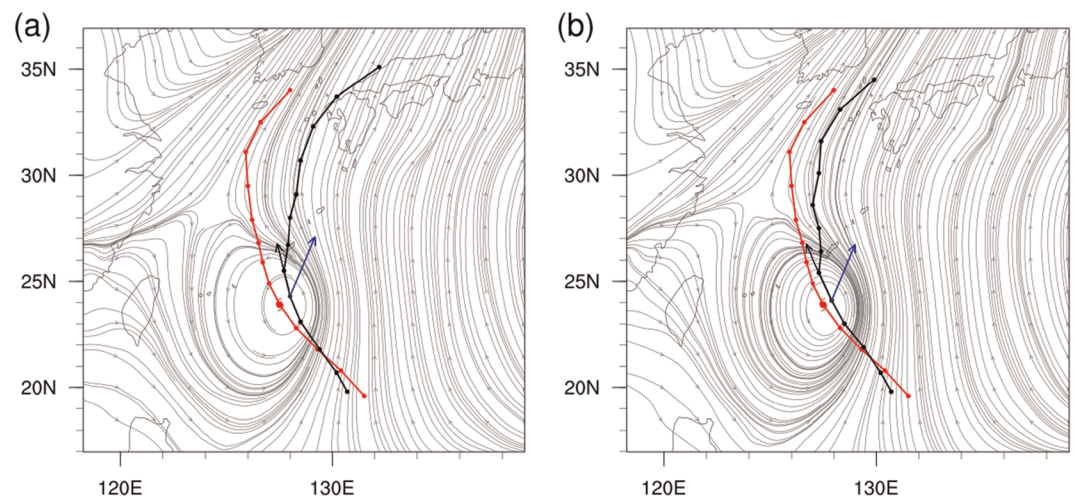

Figure 11. Same as Figure 10 but for the northwestward moving TC Chaba at 0000 UTC 3 October 2016 (24 hr forecast).
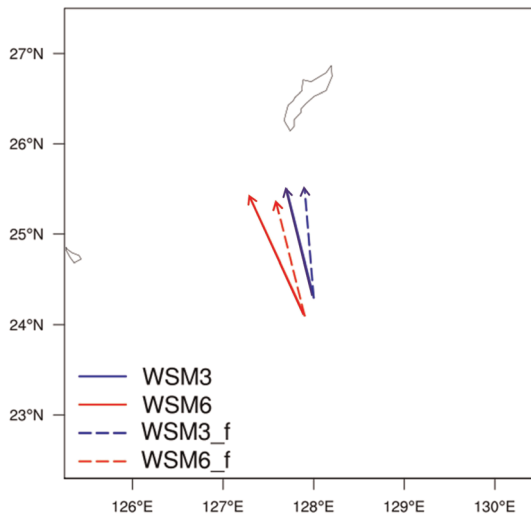
Figure 12. Motion vectors for 6 hr track forecast of β-plane (solid) and f-plane (dashed) experiments for the northwestward moving TC Chaba at 0000 UTC 3 October 2016 (24 hr forecast).

3.3. Simulated TC Motion

Here, we investigate the impact of cloud microphysics schemes on the TC motion. Generally, TC motions are determined by the large-scale environmental wind. In the tropics, an easterly wind called trade wind governs the propagation of TCs. However, in the midlatitudes, the environmental wind related to the western North Pacific subtropical high (WNPSH) plays an essential role in the northwestward movement and the recurving of TCs. In addition, the TC track can be affected by the β effect, which arises from the variation of Coriolis parameter. We hypothesize that the β effect, which is related to the TC size and intensity, impacts different TC motion in the sensitivity experiments. Theoretically, the storm size can affect the TC motion by influencing the extension and intensity of anvil clouds (Bu et al., 2014). Moreover, several studies have shown that distinct intensities, structures, and azimuthally averaged winds in the outer-core region of the TC induced due to different microphysics schemes can influence the TC motion (Sun et al., 2015) by varying the β drift in the vicinity of TC (Fiorino & Elsberry, 1989; Holland, 1984). Galarneau and Davis (2013) also indicated that the actual TC motion does not exactly equal to the surrounding steering flow due to various processes occurred in the vicinity of the storm (i.e., the storm-scale processes, the β effect generated by TC circulation itself, and so on). Thus, we mainly focus on the impact of β effect on TC movement in this subsection. To verify the β effect in each simulated TC track, we compared the steering flow in the vicinity of TC center and the simulated motion vector for 6 hr. The steering flow is defined as the averaged wind vectors at the 5–7° radius around the TC center (Chan & Gray, 1982; Liu & Xie, 2012) and at the vertical layer from 850 to 300 hPa, which have the best correlation with the TC movement (Franklin et al., 1996; Marks et al., 1992; Wu et al., 2011; Wu & Chen, 2016). Furthermore, we pay attention to the point where the differences in simulated TC track and intensity between the two runs prominently increase.

Overall, for westward moving TCs, the direction and magnitude of the motion and steering flow vectors in the two runs were mostly unaffected by the variation in simulated TC intensity and size during the entire forecast period. Figure 10 shows the motion and steering flow vectors of westward moving TC Bopha near the lifetime peak intensity (at 54 hr forecast). Although the differences in simulated TC intensity and size between the two runs are significant here, the zonal and meridional components of the motion and steering flow vectors are similar in the two runs. On the contrary, difference in the motion vector between the two runs is relatively substantial for northwestward moving TCs (Figure 11). In the case of TC Chaba among northwestward moving TCs, difference in the motion vector between the two runs is largest at 24 hr forecast when simulated TC is rapidly enhanced (see Figures 4e and 4f). The TC motion vectors point more northwestward than steering flow vectors, and the zonal and meridional components of the vector difference between the motion and steering flow vectors are −4.14 and −0.86 m s^{-1} for the WSM3 run and −5.35 and 0.1 m s^{-1} for the WSM6 run. This implies that simulated TC is affected by an additional force (i.e., the β effect) apart from the environmental steering flow wind (Li & Pu, 2008; Luo et al., 2011) to move the TC further northwestward. Also, these results suggest that the effect of β drift on TC motion could be relatively strong in the subtropics compared to the low latitudes, even if the magnitude of the β effect is relatively larger for TCs moving westward in low latitudes.

Thus, to elucidate the impact of β effect on TC movement, we conducted additional experiments, namely, f-plane sensitivity experiments with fixed Coriolis parameter around TC. These experiments were conducted only for 6 hr after the track difference between the two runs increased (i.e., 24 hr forecast). Also, to minimize the impact of modified Coriolis parameter on the surrounding environmental fields, the Coriolis parameter for the region within ±7° along the TC motion was fixed to the area-averaged value. Thus, there was no meridional change in this parameter around TC. Figure 12 shows the motion vectors acquired from f- and β-plane sensitivity experiments, and Table 2 shows the zonal and

Table 2
Comparison of U and V Components of the Vector Difference Between the Motion and Steering Flow Vectors in β- and f-Plane Sensitivity Experiments

	β plane		f plane	
	U	V	U	V
WSM3	−4.14	−0.86	−3.24	−0.82
WSM6	−5.35	0.1	−3.95	−0.45

meridional components of the difference between the motion vector and steering flow vector in β- and f-plane sensitivity experiments. The result shows that f-plane sensitivity experiments tend to simulate more eastward TC tracks compared to the β-plane experiments. Further, the differences between the f-and β-plane experiments are more prominent in the WSM6 runs as compared to that in the WSM3 runs, indicating a greater β effect related to larger TC size and stronger intensity in the former. In contrast to the motion vectors, steering flow vectors are similar in the both the experiments (not shown). This can be attributed to the fact that the large-scale environmental flow is not significantly changed in the f-plane experiments because the Coriolis parameter is only fixed in the vicinity of simulated TCs. In the f-plane experiments, the zonal and meridional components of the difference between the motion vector and steering flow vector are -3.24 and -0.82 m s^{-1} for the WSM3 run and -3.95 and -0.45 m s^{-1} for the WSM6 run. Therefore, the vector difference in the β-plane experiments is larger than that in the f-plane experiments, implying that the β effect plays a crucial role in the northwestward movement of TC.

Based on the observational studies of Chan and Gray (1982), Holland (1984), and Carr and Elsberry (1990), the magnitudes of the nonsteering component of TC motion such as β drift is ranging from 1–3 m s^{-1}, and its speed tends to increase with latitude and the TC intensity. The magnitude of β-drift vectors was reasonably simulated in the β-plane experiments, which were 0.82 m s^{-1} for the WSM3 run and 1.5 m s^{-1} for the WSM6 run in Figure 12.

4. Conclusions

We investigated the effect of cloud microphysics schemes on real-time forecasts of TCs over the WNP region. Twenty sets of forecasts for TCs, which occurred from 2012 to 2018, were conducted using the WSM3 and WSM6 cloud microphysics schemes. In most cases, the TC track and intensity forecast skills were improved in the WSM6 run. Further, the simulated TC intensity was prominently underestimated in the WSM3 run compared to that in the JTWC best track and the WSM6 run. The westward moving TCs showed similar track patterns between the two runs despite significant intensity differences. However, in northwestward moving TCs, simulated TCs in the WSM6 run tended to move more northwestward compared to that in the WSM3 run, especially during the intensification period.

The difference in simulated intensity between the two schemes resulted from the distinct hydrometeor species and their distributions in the two schemes, and different amount of diabatic heating was released from distinct cloud microphysical processes. For both the groups, simulated TCs in the WSM6 run were much stronger, and their cloud top reached to a higher level compared to that in the WSM3 run. Further, the tangential and radial winds were prominently stronger, simulated TC height and size were larger, and a stronger warm core structure was developed at the upper level in the WSM6 run. These caused a higher release of latent heat by the more sophisticated cloud microphysical process. Furthermore, the higher amount of latent heat release at the middle and upper levels enhanced the vertical motion and facilitated the intensification of the system by increasing the divergence and convergence at the upper and lower level, respectively. To clarify the reason for the different track forecasts in the two schemes, we examined the effect of TC intensity difference on the simulated TC size and therefore on the TC motion in terms of different β effect in the vicinity of TC. Consequently, the differences between the f- and β-plane sensitivity experiments are more significant in the WSM6 runs, because of the β effect, which is also function of TC size and intensity, was stronger in the WSM6 runs than the WSM3 runs. Also, the difference in the motion vector between the two schemes was more prominent in northwestward moving TCs than that in westward moving TCs. The small difference between the motion and steering wind vector means that TC motions are significantly affected by the steering wind. On the contrary, large difference between the two vectors implies that TC motion might be related to not only steering wind but also other factors. As the two groups were in different latitudinal regions, simulated TCs were affected by the distinct types of surrounding large-scale steering flow. While the trade wind governed the modulation of TC movement in the subtropical region, most of TCs moving poleward were affected by β effect as well as by midlatitude-related factors (e.g., WNPSH and westerly). This may be the reason for the difference in simulated TC motions in the two groups.

Overall, our study demonstrates that the simulated TC intensity and track are sensitive to cloud microphysics schemes in the high-resolution real-time forecast. Although the impact of cloud microphysics scheme is different in distinct latitudinal locations, the more sophisticated scheme can improve the performance of TC

track and intensity forecast compared to the simple scheme. This indicates that the track and intensity forecasts with high-resolution regional models can be improved by using the sophisticated cloud microphysics scheme when the global model used for initial and boundary conditions simulates the track of TC moving poleward. Further, the sensitivity study of TC forecast to cloud microphysics is required for global modeling to improve the TC forecast skill. This study was limited to similar cloud microphysics schemes in the WRF model (i.e., WSM family series). Therefore, to generalize the impact of cloud microphysics schemes, sensitivity tests to more schemes (e.g., double moment scheme) are required, which forms the future scope of this work.

Data Availability Statement

The Global Forecast System (GFS) forecast and analysis data for this study are taken from National Oceanic and Atmosphere Administration's National Operational Model Archive and Distribution System (NOMADS; information online at https://nomads.ncep.noaa.gov/pub/data/nccf/com/gfs/prod).

References

Bu, Y. P., Fovell, R. G., & Corbosiero, K. L. (2014). Influence of cloud-radiative forcing on tropical cyclone structure. *Journal of the Atmospheric Sciences*, *71*(5), 1644–1662. https://doi.org/10.1175/JAS-D-13-0265.1

Carr, L. E. III, & Elsberry, R. L. (1990). Observational evidence for predictions of tropical cyclone propagation relative to environmental steering. *Journal of the Atmospheric Sciences*, *47*(4), 542–546. https://doi.org/10.1175/1520-0469(1990)047<0542:OEFPOT>2.0.CO;2

Cha, D. H., Jin, C. S., Lee, D. K., & Kuo, Y. H. (2011). Impact of intermittent spectral nudging on regional climate simulation using Weather Research and Forecasting model. *Journal of Geophysical Research*, *116*, D10103. https://doi.org/10.1029/2010JD015069

Cha, D. H., & Wang, Y. (2013). A dynamical initialization scheme for real-time forecasts of tropical cyclones using the WRF model. *Monthly Weather Review*, *141*(3), 964–986. https://doi.org/10.1175/MWR-D-12-00077.1

Chan, J. C. L., & Gray, W. M. (1982). Tropical cyclone movement and surrounding flow relationships. *Monthly Weather Review*, *110*(10), 1354–1374. https://doi.org/10.1175/1520-0493(1982)110<1354:TCMASF>2.0.CO;2

Chan, J. C. L., Ko, F. M. F., & Lei, Y. M. (2002). Relationship between potential vorticity tendency and tropical cyclone motion. *Journal of the Atmospheric Sciences*, *59*(8), 1317–1336. https://doi.org/10.1175/1520-0469(2002)059<1317:RBPVTA>2.0.CO;2

Chan, K. T. F., & Chan, J. C. L. (2016). Sensitivity of the simulation of tropical cyclone size to microphysics schemes. *Advances in Atmospheric Sciences*, *33*(9), 1024–1035. https://doi.org/10.1007/s00376-016-5183-2

Chatterjee, P., Pradhan, D., & De, U. K. (2008). Simulation of hailstorm event using Mesoscale Model MM5 with modified cloud microphysics scheme. *Annales Geophysicae*, *26*(11), 3545–3555. https://doi.org/10.5194/angeo-26-3545-2008

Chen, G., Lei, X., Zhang, X., Chen, P., Yu, H., & Wan, R. (2016). Performance of tropical cyclone forecast in western North Pacific in 2015. *Tropical Cyclone Research and Review*, *5*(3), 47–57. https://doi.org/10.6057/2016TCRRh3.03

Chen, G., Yu, H., Cao, Q., & Zeng, Z. (2013). The performance of global models in TC track forecasting over the western North Pacific from 2010 to 2012. *Tropical Cyclone Research and Review*, *2*(3), 149–158. https://doi.org/10.6057/2013TCRR03.02

Chen, G., Zhang, X., Bai, L., & Wan, R. (2019). *Verification of tropical cyclone operational forecast in 2018* (pp. 1-18). Paper presented at 51th Session, ESCAP/WMO Typhoon Committee.

Chen, S. S., Price, J. F., Zhao, W., Donelan, M. A., & Walsh, E. J. (2007). The CBLAST-hurricane program and the next-generation fully coupled atmosphere-wave-ocean models for hurricane research and prediction. *Bulletin of the American Meteorological Society*, *88*(3), 311–318. https://doi.org/10.1175/BAMS-88-3-311

Chutia, L., Pathak, B., Parottil, A., & Bhuyan, P. K. (2019). Impact of microphysics parameterizations and horizontal resolutions on simulation of "MORA" tropical cyclone over Bay of Bengal using Numerical Weather Prediction Model. *Meteorology and Atmospheric Physics*, *131*(5), 1483–1495. https://doi.org/10.1007/s00703-018-0651-0

Deshpande, M. S., Pattnaik, S., & Salvekar, P. S. (2012). Impact of cloud parameterization on the numerical simulation of a super cyclone. *Annales Geophysicae*, *30*(5), 775–795. https://doi.org/10.5194/angeo-30-775-2012

Dudhia, J. (1989). Numerical study of convection observed during the winter monsoon experiment using a mesoscale two-dimensional model. *Journal of the Atmospheric Sciences*, *46*(20), 3077–3107. https://doi.org/10.1175/1520-0469(1989)046<3077:NSOCOD>2.0.CO;2

Emanuel, K. (1986). An air-sea interaction theory for tropical cyclones. Part I: Steady-state maintenance. *Journal of the Atmospheric Sciences*, *43*(6), 585–605. https://doi.org/10.1175/1520-0469(1986)043<0585:AASITF>2.0.CO;2

Fiorino, M., & Elsberry, R. L. (1989). Some aspects of vortex structure related to tropical cyclone motion. *Journal of the Atmospheric Sciences*, *46*(7), 975–990. https://doi.org/10.1175/1520-0469(1989)046<0975:SAOVSR>2.0.CO;2

Franklin, J. L., Feuer, S. E., Kaplan, J., & Aberson, S. D. (1996). Tropical cyclone motion and surrounding flow relationships: Searching for beta gyres in omega dropwindsonde datasets. *Monthly Weather Review*, *124*(1), 64–84. https://doi.org/10.1175/1520-0493(1996)124<0064:TCMASF>2.0.CO;2

Galarneau, T. J., & Davis, C. A. (2013). Diagnosing forecast errors in tropical cyclone motion. *Monthly Weather Review*, *141*(2), 405–430. https://doi.org/10.1175/MWR-D-12-00071.1

Guimond, S. R., Bourassa, M. A., & Reasor, P. D. (2011). A latent heat retrieval and its effects on the intensity and structure change of Hurricane Guillermo (1997). Part I: The algorithm and observations. *Journal of the Atmospheric Sciences*, *68*(8), 1549–1567. https://doi.org/10.1175/2011JAS3700.1

Holland, G. J. (1984). Tropical cyclone motion: A comparison of theory and observation. *Journal of the Atmospheric Sciences*, *41*(1), 68–75. https://doi.org/10.1175/1520-0469(1984)041<0068:TCMACO>2.0.CO;2

Hong, S. Y., Dudhia, J., & Chen, S. H. (2004). A revised approach to ice microphysical processes for the bulk parameterization of clouds and precipitation. *Monthly Weather Review*, *132*(1), 103–120. https://doi.org/10.1175/1520-0493(2004)132<0103:ARATIM>2.0.CO;2

Hong, S. Y., & Lim, J. O. J. (2006). The WRF single-moment 6-class microphysics scheme (WSM6). *Journal of the Korean Meteorological Society*, *42*(2), 129–151.

Hong, S. Y., Noh, Y., & Dudhia, J. (2006). A new vertical diffusion package with an explicit treatment of entrainment processes. *Monthly Weather Review*, *134*(9), 2318–2341. https://doi.org/10.1175/MWR3199.1

Kain, J. S. (2004). The Kain-Fritsch convective parameterization: An update. *Journal of Applied Meteorology*, *43*(1), 170–181. https://doi.org/10.1175/1520-0450(2004)043<0170:TKCPAU>2.0.CO;2

Kanase, R. D., & Salvekar, P. S. (2015). Effect of physical parameterization schemes on track and intensity of cyclone LAILA using WRF model. *Asia-Pacific Journal of Atmospheric Sciences*, *51*(3), 205–227. https://doi.org/10.1007/s13143-015-0071-8

Kitoh, A., Ose, T., Kurihara, K., Kusunoki, S., & Sugi, M. (2009). Projection of changes in future weather extremes using super-high-resolution global and regional atmospheric models in the KAKUSHIN Program: Results of preliminary experiments. *Hydrological Research Letters*, *3*, 49–53. https://doi.org/10.3178/hrl.3.49

Knabb, R. D., Rhome, J. R., & Brown, D. P. (2006). Tropical cyclone report: Hurricane Katrina, 23–30 August 2005. *National Hurricane Center*.

Knutson, T. R., McBride, J. L., Chan, J., Emanuel, K., Holland, G., Landsea, C., et al. (2010). Tropical cyclones and climate change. *Nature Geoscience*, *3*(3), 157–163. https://doi.org/10.1038/ngeo779

Leroux, M. D., Wood, K., Elsberry, R. L., Cayanan, E. O., Hendricks, E., Kucas, M., et al. (2018). Recent advances in research and forecasting of tropical cyclone track, intensity, and structure at landfall. *Tropical Cyclone Research and Review*, *7*(2), 85–105. https://doi.org/10.6057/2018TCRR02.02

Li, X., & Pu, Z. (2008). Sensitivity of numerical simulation of early Rapid Intensification of Hurricane Emily (2005) to cloud microphysical and planetary boundary layer parameterizations. *Monthly Weather Review*, *136*(12), 4819–4838. https://doi.org/10.1175/2008MWR2366.1

Liang, X. Z., Xu, M., Yuan, X., Ling, T., Choi, H. I., Zhang, F., et al. (2012). Regional Climate-Weather Research and Forecasting model. *Bulletin of the American Meteorological Society*, *93*(9), 1363–1387. https://doi.org/10.1175/BAMS-D-11-00180.1

Liu, B., & Xie, L. (2012). A scale-selective data assimilation approach to improving tropical cyclone track and intensity forecasts in a limited-area model: A case study of Hurricane Felix (2007). *Weather and Forecasting*, *27*(1), 124–140. https://doi.org/10.1175/WAF-D-10-05033.1

Liu, H. Y., & Tan, Z. M. (2016). A dynamical initialization scheme for binary tropical cyclones. *Monthly Weather Review*, *144*(12), 4787–4803. https://doi.org/10.1175/MWR-D-16-0176.1

Luo, Z., Davidson, N. E., Ping, F., & Zhou, W. (2011). Multiple-scale interactions affecting tropical cyclone track changes. *Advances in Mechanical Engineering*, *3*, 782590. https://doi.org/10.1155/2011/782590

Marks, F. D. Jr., Houze, R. A. Jr., & Gamache, J. F. (1992). Dual-aircraft investigation of the inner core of Hurricane Norbert. Part I: Kinematic structure. *Journal of the Atmospheric Sciences*, *49*(11), 919–942. https://doi.org/10.1175/1520-0469(1992)049<0919:DAIOTI>2.0.CO;2

Miguez-Macho, G., Stenchikov, G. L., & Robock, A. (2005). Regional climate simulations over North America: Interaction of local processes with improved large-scale flow. *Journal of Climate*, *18*(8), 1227–1246. https://doi.org/10.1175/JCLI3369.1

Miyoshi, T., Sato, Y., & Kadowaki, T. (2010). Ensemble Kalman filter and 4D-Var intercomparison with the Japanese operational global analysis and prediction system. *Monthly Weather Review*, *138*(7), 2846–2866. https://doi.org/10.1175/2010MWR3209.1

Mlawer, E. J., Taubman, S. J., Brown, P. D., Iacono, M. J., & Clough, S. A. (1997). Radiative transfer for inhomogeneous atmospheres: RRTM, a validated correlated-k model for the longwave. *Journal of Geophysical Research*, *102*(D14), 16,663–16,682. https://doi.org/10.1029/97jd00237

Mohanty, U. C., Osuri, K. K., Routray, A., Mohapatra, M., & Pattanayak, S. (2010). Simulation of Bay of Bengal tropical cyclones with WRF model: Impact of initial and boundary conditions. *Marine Geodesy*, *33*(4), 294–314. https://doi.org/10.1080/01490419.2010.518061

Moon, J., Cha, D. H., Lee, M., & Kim, J. (2018). Impact of spectral nudging on real-time tropical cyclone forecast. *Journal of Geophysical Research: Atmospheres*, *123*, 12,647–12,660. https://doi.org/10.1029/2018JD028550

Mooney, P. A., Mulligan, F. J., & Fealy, R. (2013). Evaluation of the sensitivity of the Weather Research and Forecasting model to parameterization schemes for regional climates of Europe over the period 1990–95. *Journal of Climate*, *26*(3), 1002–1017. https://doi.org/10.1175/JCLI-D-11-00676.1

Mukhopadhyay, P., Taraphdar, S., & Goswami, B. N. (2011). Influence of moist processes on track and intensity forecast of cyclones over the north Indian Ocean. *Journal of Geophysical Research*, *116*, D05116. https://doi.org/10.1029/2010JD014700

Noh, Y., Cheon, W. G., Hong, S. Y., & Raasch, S. (2003). Improvement of the K-profile model for the planetary boundary layer based on large eddy simulation data. *Boundary-Layer Meteorology*, *107*(2), 401–427. https://doi.org/10.1023/A:1022146015946

Nolan, D. S., Zhang, J. A., & Stern, D. P. (2009). Evaluation of planetary boundary layer parameterizations in tropical cyclones by comparison of in situ observations and high-resolution simulations of Hurricane Isabel (2003). Part I: Initialization, maximum winds, and the outer-core boundary layer. *Monthly Weather Review*, *137*(11), 3651–3674. https://doi.org/10.1175/2009MWR2785.1

Pattnaik, S., & Krishnamurti, T. N. (2007). Impact of cloud microphysical processes on hurricane intensity, Part 2: Sensitivity experiments. *Meteorology and Atmospheric Physics*, *97*(1–4), 127–147. https://doi.org/10.1007/s00703-006-0248-x

Rao, G. V., & Rao, D. B. (2003). A review of some observed mesoscale characteristics of tropical cyclones and some preliminary numerical simulations of their kinematic features. *PROCEEDINGS-INDIAN NATIONAL SCIENCE ACADEMY PART A*, *69*(5), 523–542.

Skamarock, W. C., Klemp, J. B., Dudhia, J., Gill, D. O., Barker, D. M., Duda, M. G., et al. (2008). A description of the advanced research WRF Version 3. In *NCAR Tech. Note NCAR/TN-475+ STR*.

Srinivas, C. V., Venkatesan, R., Rao, D. B., & Prasad, D. H. (2007). Numerical simulation of Andhra severe cyclone (2003): Model sensitivity to the boundary layer and convection parameterization. In *Atmospheric and Oceanic* (pp. 1465–1487). Basel: Birkhäuser.

Stensrud, D. J. (2009). *Parameterization schemes: Keys to understanding numerical weather prediction models*. Cambridge: Cambridge University Press.

Sun, Y., Zhong, Z., & Lu, W. (2015). Sensitivity of tropical cyclone feedback on the intensity of the Western Pacific subtropical high to microphysics schemes. *Journal of the Atmospheric Sciences*, *72*(4), 1346–1368. https://doi.org/10.1175/JAS-D-14-0051.1

Tao, W. K., Shi, J. J., Chen, S. S., Lang, S., Lin, P. L., Hong, S. Y., et al. (2011). The impact of microphysical schemes on hurricane intensity and track. *Asia-Pacific Journal of Atmospheric Sciences*, *47*(1), 1–16. https://doi.org/10.1007/s13143-011-1001-z

Warner, T. T. (2010). *Numerical weather and climate prediction*. Cambridge: Cambridge University Press. https://doi.org/10.1017/CBO9780511763243

Wu, L., & Chen, X. (2016). Revisiting the steering principal of tropical cyclone motion in a numerical experiment. *Atmospheric Chemistry and Physics*, *16*(23), 14,925–14,936. https://doi.org/10.5194/acp-16-14925-2016

Wu, L., Liang, J., & Wu, C. C. (2011). Monsoonal influence on Typhoon Morakot (2009). Part I: Observational analysis. *Journal of the Atmospheric Sciences*, *68*(10), 2208–2221. https://doi.org/10.1175/2011JAS3730.1

Zhang, J. A., Gopalakrishnan, S., Marks, F. D., Rogers, R. F., & Tallapragada, V. (2012). A developmental framework for improving hurricane model physical parameterizations using aircraft observations. *Tropical Cyclone Research and Review*, *1*(4), 419–429. https://doi.org/10.6057/2012TCRR04.01

Zhu, T., & Zhang, D. L. (2006). Numerical simulation of Hurricane Bonnie (1998). Part II: Sensitivity to varying cloud microphysical processes. *Journal of the Atmospheric Sciences*, *63*(1), 109–126. https://doi.org/10.1175/JAS3599.1

Zou, X., Wu, Y., & Ray, P. S. (2010). Verification of a high-resolution model forecast using airborne Doppler radar analysis during the rapid intensification of Hurricane Guillermo. *Journal of Applied Meteorology and Climatology*, *49*(4), 807–820. https://doi.org/10.1175/2009JAMC2182.1